Published in final edited form as:
NMR Biomed. 2015 January ; 28(1): 1–8. doi:10.1002/nbm.3216.

CEST Signal at 2ppm (CEST@2ppm) from Z-Spectral Fitting Correlates with Creatine Distribution in Brain Tumor

Kejia Cai[1], **Anup Singh**[2], **Harish Poptani**[3], **Weiguo Li**[4,5], **Shaolin Yang**[6], **Yang Lu**[1], **Hari Hariharan**[2], **Xiaohong J. Zhou**[1], and **Ravinder Reddy**[2]

[1]Department of Radiology, University of Illinois College of Medicine, Chicago, IL, USA

[2]Center for Magnetic Resonance and Optical Imaging (CMROI), Department of Radiology, University of Pennsylvania, Philadelphia, PA, USA

[3]Molecular Imaging Labs, Department of Radiology, University of Pennsylvania, Philadelphia, PA, USA

[4]Research Resource Center, Department of Bioengineering, University of Illinois College of Medicine, Chicago, IL, USA

[5]Department of Radiology, Northwestern University, Chicago, IL, USA

[6]Department of Psychiatry and Radiology, University of Illinois College of Medicine, Chicago, IL, USA

Abstract

In general, multiple components such as water direct saturation (DS), magnetization transfer (MT), chemical exchange saturation transfer (CEST) and aliphatic nuclear overhauser effect (NOE) contribute to Z-spectrum. The conventional CEST quantification method based on asymmetrical analysis may lead to quantification errors due to the semi-solid MT asymmetry and the aliphatic NOE effect located on single side of the Z-spectrum. Fitting individual contributors to the Z-spectrum may improve the quantification of each component. In this study, we aim to characterize the multiple exchangeable components from an intracranial tumor model using a simplified Z-spectral fitting method. In this method, the Z-spectrum acquired at low saturation RF amplitude (50 Hz) was modeled as the summation of five Lorentzian functions that correspond to NOE, MT effect, bulk water, amide proton transfer (APT) effect and a CEST peak located at +2ppm, called CEST@2ppm. With the pixel-wise fitting, the regional variation of these five components in the brain tumor and the normal brain tissue were quantified and summarized. Increased APT effect, decreased NOE and reduced CEST@2ppm were observed in the brain tumor compared to the normal brain tissue. Additionally, the CEST@2ppm decreased with tumor progression. The CEST@2ppm was found to correlate with the creatine concentration quantified with proton magnetic resonance spectroscopy (^{1}H-MRS). Based on the correlation curve, the creatine contribution to the CEST@2ppm was quantified. The CEST@2ppm signal could be a

Address for Correspondence: Kejia Cai, PhD, 3T MR Research Program, Center for MR Research, Department of Radiology, University of Illinois College of Medicine, Chicago, IL, 60612, Tel: (312) 413-0091, Fax: (312) 355-1637, kcai@uic.edu.

"The authors disclose no potential conflicts of interest."

novel imaging surrogate for *in vivo* creatine, the important bioenergetics marker. Given its noninvasive nature, this CEST MRI method may have broad applications in cancer bioenergetics.

Keywords

chemical exchange saturation transfer (CEST); amide proton transfer (APT); nuclear overhauser enhancement (NOE); brain tumor; magnetic resonance spectroscopy (MRS); creatine

Introduction

Primary brain tumors have a wide range of different histological subtypes. Gliomas account for approximately 77% of primary malignant brain tumors and thus, they are most frequently diagnosed primary brain tumors with predominance of astrocytomas. (1,2). Although the prognosis for patients with high-grade gliomas is relatively poor, the choice of treatment protocol can have a significant impact on survival. Magnetic resonance imaging (MRI) helps in predicting clinical outcome and hence contributes to individualized treatment planning. Previous studies have shown that MRI-derived parameters help in predicting clinical outcomes (3,4). Conventional MRI (T_1, T_2 weighted) and dynamic contrast enhanced MRI (DCE-MRI) are useful for identifying soft-tissue morphological changes in patients with gliomas (5–9). Alternative MRI methods based on noninvasive and endogenous contrasts are in great need to probe tumor metabolism, determine tumor grade and guide treatment planning.

MRI on the basis of the chemical exchange saturation transfer (CEST) effect from amine, amide, sulfhydryl and hydroxyl protons associated with endogenous metabolites has been shown to provide imaging maps of metabolites in tissue noninvasively. CEST MRI has been previously exploited to measure amide protons (amide proton transfer or APT) (10), liver glycogen (11), cartilage glycosaminoglycans(12), brain myo-inositol(13), Glutamate (14), glucose(15,16) and others (17) with a high spatial resolution.

The CEST contrast is generally quantified from the magnetization transfer ratio (MTR) asymmetry as in the following formula (10–14,18):

$$\mathrm{CEST}=100^{*}(\mathrm{M}_{-}-\mathrm{M}_{+})/\mathrm{M}_{0} \quad (1)$$

where M_- at the opposite side of the Z-spectrum serves as the reference signal for M_+, the water signal when saturation is turned “on” at a particular downfield offset of Z-spectrum. M_0 is the overall water signal when saturation is “off” and is used for normalization. In some cases, M_- may also be used for normalization (18). By subtracting M_+ from M_-, contaminations from magnetization transfer (MT) and water direct saturation (DS) effects are presumably removed, leaving only the CEST effect from metabolites.

However, this conventional CEST quantification method may lead to errors due to the semi-solid MT asymmetry (19) and the reported aliphatic nuclear overhauser enhancement (NOE) (12,20–22) located predominantly in the upfield of Z-spectrum. To improve the CEST quantification, Z-spectral fitting methods have been investigated. Given the Z-spectral

fittings based on Bloch-McConnell equations are strongly dependent on starting values, and lack of accuracy and reliability (23), Lorentzian functions were recently used to fit Z-spectrum as a combination of three components: MT, DS and the remaining component from metabolites (24). More recently, Z-spectrum was fitted as a sum of four Lorentzian functions (DS, Amide, Amine and NOE), assuming constant MT across the spectrum due to the use of low saturation power and short duration (25).

A recent study revealed a total of five contributors to the Z-spectra, including water DS, MT effect, amide proton transfer effect, aliphatic NOE and a +2ppm peak, called CEST@2ppm hereafter (22). A comprehensive quantification of all these five components *in vivo* has not yet been performed. In addition, although the earlier literature hypothesized that the CEST@2ppm was due to mobile lipids or amide protons associated with proteins (26,27) or amine protons (25,28), this assignment is not quantitatively determined (22).

In this study, we evaluated CEST-MRI for characterizing the exchangeable components in an intracranial tumor model through a simplified Z-spectral fitting method. CEST@2ppm was particularly investigated and its contribution from creatine was quantitatively studied.

MATERIALS AND METHODS

All animal experiments were performed according to approved protocols by the Institutional Animal Care and Use Committee (IACUC) at the University of Pennsylvania, USA. Tumor cells (9L gliosarcoma) were implanted into Fisher rat brains using well-established methods (14,29). Longitudinal imaging studies were performed on tumor-bearing rats (n=5) at 3 and 4 weeks post tumor implantation with a 9.4T horizon Varian small-animal MRI scanner and a 35 mm inner-diameter rat head-coil (M2M imaging, Cleveland, OH). One rat died before reaching the second imaging time-point. The average tumor volume was 21.3±2.7 mm^3 and 151.1±29.5 mm^3 for the 1^{st} and 2^{nd} imaging time-points respectively. Tumor volume was obtained as 1/2 $a \times b^2$, where a is the long axis and b is the short axis of tumor central slices based on the anatomical T_2-weighted images.

MRI and Image Processing

T_2-weighted fast spin-echo multi-slice images were acquired for localizing brain tumors with imaging parameters: TR/TE= 2000/40 ms, number of slices = 10, slice thickness = 2 mm. Z-spectra (up to 100 ppm) from the tumor central slice were acquired using 50Hz continuous-wave saturation RF pulse lasting for 3s followed by single shot Fast Low-Angle SHot imaging (FLASH) readout (14) (shot TR=11.4s and readout TR/TE=6/3 ms). Other imaging parameters are: field of view = 30 × 30 mm^2, matrix = 128 × 128, slice thickness = 2 mm and 2 averages. The entire Z-spectrum contains a total of 61 images acquired at various saturation offsets, including −5 to 5 ppm in an increment of 0.25 ppm, ±6 to ±12 ppm in an increment of 1 ppm, ±25 ppm, ±50 ppm and ±100 ppm. Total imaging time for the entire Z-spectrum was about 24 min. Following Z-spectra acquisition, images for B_0 and B_1 mapping were acquired as described in a previous study (14). A B_0 field map was obtained from three complex (magnitude and phase) gradient echo images with TE = 3.0, 3.5, 4.0 ms. Following phase unwrapping, the averaged ratio of phase difference over TE difference rendered the B_0 frequency offset. Images for B_1 field mapping were acquired

using a 2D single shot FLASH readout sequence with excitatory square pulses followed by a spoiler gradient, readout TR/TE = 6/3 ms, shot TR = 9 s and 128 × 128 image matrix. Two image obtained with flip angles of 30° and 60° were used to quantify the pixel-wise flip angle or relative B_1 map based on the relationship of MR signal as a cosine function of flip angle.

Before the fitting, Z-spectra within ±12ppm range were normalized by the signal at +100 ppm and center-corrected using B_0 field map. Z-spectra were flipped to be $100*(1-M_z/M_0)$ and then fitted with a sum of five Lorentzian functions corresponding to NOE, MT effect, bulk water, the CEST@2ppm and APT effect located at around −3.2, −1.5, 0 and 2.0 and 3.6 ppm, respectively as shown in the following equations.

$$Z(w)=100-\sum_1^5 L_n(w) \quad (2)$$

$$L(w)=\frac{A}{1+4*\left(\frac{w-w0}{lw}\right)^2} \quad (3)$$

where *w* is the frequency offset related to water resonance. *A*, w_0 and *lw* are respectively the amplitude, center frequency offset and line width of any CEST peak.

The nonlinear constrained fitting routine “lsqcurvefit” was performed in MATLAB 7.0 (Natick, MA, USA). The fitting parameters were flexibly constrained, allowing for peak amplitudes to vary from 1/100 to 10 times of the initial values, peak line-widths 1/2 to 2 times of the initial values and the peak frequency offsets ±10% of the corresponding line-widths. After this first round of fitting, bulk water and MT peaks as the two dominant components were subtracted from the Z-spectra and a secondary fitting of the remaining three peaks was performed. In the secondary fitting, the remaining Z-spectrum data were locally interpolated by two times around the top of the three peaks so that the fitting would not be driven by the data points near boundaries. The initial values of the secondary fitting were the results from the first fitting and were more tightly constrained to allow peak amplitudes to vary from 1/10 to 5 times of initials, line-widths 1/2 to 1.5 times of initials, and frequency offsets between ±0.05 ppm around initials. Goodness of fit (R^2) was calculated on a pixel-wise basis after the secondary fitting.

MR spectroscopy

Localized shimming of voxels of interest in the tumor and the contralateral normal brain tissue from the normal thalamus was performed using the single voxel Point-RESolved Spectroscopy (PRESS) (30) sequence and with water suppression using VAriable Pulse power and Optimized Relaxation delays (VAPOR) (31). Other acquisition parameters were: voxel size = 3 × 1.5 × 2 mm^3, TR/TE= 3000/13 ms, 256 averages. Each water suppressed spectrum took about 13 min to acquire. The corresponding water reference spectra were also acquired using the same parameters except without water suppression and 32 averages. The acquisition of each water reference spectrum took about 1.5 min.

The acquired spectra were processed using the time domain fitting program MRUI (32,33). In brief, water suppressed or water reference data were read, apodized with a 20 Hz Gaussian function, phase corrected, and fitted with Lorentzian functions using the MRUI conventional method called the Advanced Method for Accurate, Robust and Efficient (Amares). The integration of the creatine peak was generated after fitting and normalized by the water reference integral for the quantification of creatine concentration.

Statistical analysis

Paired one-tailed Student's t-test was used to compare the fitted peak integrals or amplitudes from tumor and the contralateral normal brain tissue. The same test was also used to compare the fitted CEST@2ppm integral at two different imaging time points. The difference was consider to be significant if $p<0.05$. Values are reported as Mean ± Standard Error (SE). Creatine concentrations quantified by MRS and CEST@2ppm peak integrals from tumors and normal brain tissues were pooled together for a Pearson's correlation test. Pearson's r and p values were calculated.

Results

In Figure 1A, representative Z-spectra from brain tumor and normal brain tissue show the bulk water peak, an underlying broad MT component, and three additional peaks located at round −3.2, +2.0 and +3.6 ppm, corresponding to aliphatic NOE (22), the CEST@2ppm, and APT effect (34), respectively. Due to the contaminations from the NOE and the semi-solid MT asymmetry effect, CEST contrast maps at +2ppm and +3.6ppm calculated using the conventional asymmetrical analysis presented mostly negative values across the brain as shown in Figure 1C–D. Figure 2 demonstrates the two steps of Z-spectral fitting process with five and three Lorentzian functions, respectively. The initial values for parameters to fit and their average fitted values from the first and second round of fittings were listed in Table 1. An increased APT and decreased CEST@2ppm integrals (or peak areas) were observed in the tumor compared to the normal brain tissue (Figure 2C,D). The peak amplitude of the CEST@2ppm didn't appear to change in tumor, while its integral reduced by over 50% due to the narrower line-width from tumor compared to the normal brain tissue (Figure 2C–D).

Fitting the Z-spectra pixel by pixel provided us the frequency offset, amplitude, line-width and integral maps of the five peaks, including the CEST@2ppm and APT peaks (Figure 2F–G). Most pixels were fitted with $R^2 >0.95$ except those from a small edematous region, where the metabolite levels were negligible. Figure 3 shows the pixel-wise fitted integral, chemical shift, linewidth and amplitude maps of the five components contributing to the Z-spectra. As summarized in Figure 4, fitted peak integrals of NOE (tumor 68.0±4.3 vs contralateral 92.1±5.3 ppm%, $p<0.005$), MT (tumor 575.6±15.0 vs contralateral 982.0±31.9 ppm%, $p<0.0001$), bulk water (tumor 165.7±3.5 vs contralateral 131.0±2.5 ppm%, $p<0.005$), +2ppm (tumor 32.5±4.7 vs contralateral 55.0±9.0 ppm%, $p<0.05$) and APT (tumor 13.7±0.6 vs contralateral 5.5±0.6 ppm%, $p<0.001$) were all significantly different between the tumor and the contralateral brain tissue. Similarly, fitted amplitudes were all significantly different, including NOE (tumor 12.4±0.4 vs contralateral 14.6±0.4 ppm%,

p<0.005), MT (tumor 16.9±0.7 vs contralateral 26.4±0.8 ppm%, p<0.0005), water (tumor 76.8±0.5 vs contralateral 63.9±1.0 ppm%, p<0.0001) and APT (tumor 7.4±0.2 vs contralateral 4.0±0.2 ppm%, p<0.001), except for the CEST@2ppm (tumor 9.8±0.8 vs contralateral 10.8±0.9 ppm%, 0.05<p<0.1).

As the tumor progressed in size (from the 1st to the 2nd imaging time point), CEST@2ppm integral of tumor further decreased (32.5±4.7 vs 28.5±3.4 ppm%, p<0.05) as demonstrated in Figure 5A–B. This decrease in CEST@2ppm integral correlated with the creatine concentrations quantified with MR spectroscopy (Figure 5C). Correspondingly, creatine concentration decreased from 6.3±1.0 mM at imaging time point 1 to 4.2±0.3 mM at imaging time point 2.

The linear correlation of the CEST@2ppm integrals with the corresponding creatine concentrations rendered a ratio of 3.95 ppm% per mM creatine (Figure 6) and Pearson's r of 0.82 (p<0.001). The intercept of 12.26 ppm% indicated that other contributions to CEST@2ppm were equivalent to about 3 mM creatine.

Discussion

CEST contrast based on conventional asymmetric analysis receives contaminations from the intrinsic MT asymmetry and aliphatic NOE effect. Given mostly negative CEST contrast at +2 ppm and +3.6 ppm were observed across the brain using the conventional asymmetrical analysis, the observed contrasts were dominated by the intrinsic MT asymmetry and aliphatic NOE effect under the imaging conditions. Hence fitting individual contributions to Z-spectrum is necessary.

With limited range of saturation offset, super Lorentzian fitting of the MT contribution (35) to Z spectrum may be highly dependent on initial values (23,24). MT pool within a small range of Z spectrum can also be approximately modeled by a Lorentzian function (23). Recently, Zaiss et al. proposed to use Lorentzian functions to fit Z spectra (23,24). In this study, we fitted Z-spectra with five Lorentzian-shaped peaks to separate the contributions from the semi-solid MT asymmetry and aliphatic NOE that contaminate the conventional asymmetric analysis.

The pixel by pixel Lorentzian fitting demonstrates good performance in our study as suggested by high R_2 values. Features observed from the fitted maps agree with the literatures. For example, we observed decreased MTR (36,37), increased water content (38) and increased APT (10) in tumor compared to normal brain tissue. Consistent with the literature, we also observed a negative offset of semi-solid MTR (39) located at around −2ppm from water. The fitted MT linewidths (normal brain: 25.8±0.9 ppm, tumor: 23.6±1.1 ppm) are also reasonable due to the typical short bound water T_2 in the order of microsecond (39,40). The CEST@2ppm coarsely correlated to MT distribution, while APT showed reversely correlated pattern with MT. This indicates that CEST@2ppm, APT and MT based on different contrast mechanisms can all reflect tumor pathology while in varied aspects.

As shown in our results, the APT integral increases in tumor due to an increase in both its linewidth and amplitude. This could indicate that there are more variety and higher

concentration of amide protons in tumor since APT contrast origins from various amide proton populations centered at slightly different resonances.

On the other hand, we observed the reduced CEST@2ppm peak integral in the tumor compared to the normal tissue, which is presumably due to the reduction of peak linewidth. The linewidth of a CEST peak is dependent on multiple factors, including the saturation amplitude, T_2 of exchangeable protons, static field inhomogeneity and the proton exchange rate (related to pH). The reduced linewidth of the CEST@2ppm peak in tumor is most likely due to the increased overall tissue T_2 instead of pH reduction. pH often reduces in tumor extracellular space (41). CEST effect from intracellular metabolites, such as creatine, should not be significantly affected. Given there were insignificant difference in the CEST@2ppm peak amplitudes, the CEST@2ppm peak integral provided higher contrast between tumor and normal brain tissue. CEST peak integral which incorporates information from both peak amplitude and linewidth can be an alternative signal sensitive to tissue microenvironmental and molecular changes. Previously, the CEST@2ppm peak was tentatively assigned to glutamine and protein (26). However, it is recently proven that CEST effect from glutamine's fast-exchanging amine protons cannot be detected at physiological and tumor pH (14,42). Furthermore, the fact that APT from proteins increased while the CEST@2ppm decreased in tumor indicates proteins may not be the major contribution to the CEST@2ppm. Recently, researchers intended to assign CEST@2ppm to amine protons in general (25,28). Particularly, Jin et al. has also mentioned the contribution from creatine amine protons (28). However, no studies have quantitatively investigated this assignment.

Because, among the major brain and brain tumor metabolites with slow to intermediate exchangeable protons, only creatine amine or guanidinium protons exhibit CEST effect centered at +2ppm from water (43–45), we suggest that creatine is the major contributor to the CEST@2ppm, consistent to early studies (46,47). For example, Arus et al. assigned the observed 6.7 ppm (or 2ppm from water resonance) peak in intact muscle MR spectrum to creatine (46). A recently published paper on creatine CEST and its application in myocardial infarct also demonstrated that the 2ppm peak is mainly due to creatine (48).

It is well documented that creatine plays a critical role in tissue bioenergetics. creatine provides phosphate through phospho-creatine (PCr) for adenosine triphosphate (ATP) synthesis in the cell energy requirement (5,49,50). In 1939, Belitzer and Tsybakova showed that oxygen consumption increases strongly in the presence of creatine (51), whose concentration became an important kinetic parameter in the regulation of respiration and energy fluxes. Our MR spectroscopy data is consistent to the previous findings that tumor has reduced creatine (52–54) and tumor creatine further reduces with tumor progression (55) presumably due to elevated energy deficiency. The linear correlation (Figure 6) between creatine concentrations (quantified with MRS) with the CEST@2ppm integral further supports that creatine may be a major contributor to CEST@2ppm. The intercept of 12.26 ppm% indicates that there are other unknown factors (equivalent to about 3 mM creatine) that contribute to the CEST@2ppm integral. These contributing factors could include amine or amide protons associated with amino acids, peptides and proteins. The contribution from these factors may vary between different tissue types, such as between tumor and normal brain tissue. Precisely determining these differences is challenging and remains to be

investigated. Hence, using the CEST@2ppm as the indicator of creatine requires the estimation of the correlation coefficient similar to what we demonstrated in Figure 6.

Mapping *in vivo* creatine spatial distribution is important for investigating tissue bioenergetics. Magnetic resonance spectroscopic imaging (MRSI) of creatine has been applied for this purpose (5). However, MRSI is limited by its poor spatial resolution (>mm) and long acquisition time. CEST@2ppm, once calibrated, might be a novel imaging method for mapping *in vivo* creatine distribution.

However, there are a few issues that worth discussion. Firstly, the tumor affected region defined by the creatine map is sometimes slightly larger than the conventional MRI contrasts (e.g. APT, MT or proton density). This may indicate that the surrounding tissue is also metabolically affected by the presence of tumor. Secondly, this method though provides more and accurate information, requires data from entire Z-spectrum and hence longer imaging time. Thirdly, water signal was used as a reference in MRS quantification. In tumors, the extracellular water content increases. Since water content increase in tumor extracellular space is associated with an increase in extracellular volume and the overall tissue volume, normalizing with water signal is somewhat equivalent to normalizing with tissue volume. However, given that water occupies slightly less percentage of intracellular volume than extracellular volume, ignoring this difference may create systematic errors in quantification. However, this is difficult to calibrate due to many unknown factors, including the ratio of intracellular to extracellular volumes. In a similar fashion, although the contributions from metabolites such as creatine are mainly from intracellular space, CEST contrasts also provide averaged information from overall tissue. Hence, the correlation between CEST signals with MRS quantifications should still be valid.

Fourthly, the exchange rate of creatine amine protons was estimated with large inconsistencies from the literatures (from a couple of hundreds to over one thousand) (43,56–58). It is hard to quantify the *in vivo* exchange rate experimentally. Similarly, the estimation of its labeling efficiency is challenging and requires the values that are not experimentally accessible, such as exchange rates, intrinsic T_1, T_2 of both bulk water and exchangeable protons. Sometimes these values were estimated (56). However, labeling efficiency can be much different by estimating T_2 of solute exchangeable protons from 0.1 to 0.001 s.

Fifthly, in the current fitting method, a total of five peaks were fitted because they are the visible ones in the collected Z-spectra. Incorporating an invisible peak into the fitting may lead to fitting errors unless there is sufficient prior knowledge. The visibility of a CEST peak predominantly depends on the proton concentration, exchange rate and frequency offset. In general, the exchangeable protons with longer T_2, slower exchange rate and larger offset from water resonance are more likely to form a visible CEST peak under a prolonged saturation pulse with relatively low amplitude. The visibility of a CEST peak in Z-spectrum also depends on many other factors, including field strength, static field homogeneity, saturation amplitude and duration, and the acquisition step size of the Z-spectrum. For example, by changing the imaging parameters to enhance the Z-spectrum resolution, finer structure of Z-spectrum with more visible peaks may be seen. Hence, fitting Z-spectrum

with five components may not always be validated under other imaging conditions. It is possible that the relatively fast exchanging components may also be partially labeled. Given that they do not visibly show as peaks. During the fitting, they may be treated as part of MT or water peak. Lastly, changes in tissue T_1, T_2 and spillover effect may affect the quantification of CEST peaks in complicated ways. In contrast to the published methods (56,59), our approach is not able to correct those factors.

Nevertheless, given its noninvasive nature, CEST MRI for creatine imaging may have broad implications in cancer bioenergetics.

Acknowledgement

We gratefully acknowledge stimulating discussions with Drs. Mohammad Haris, Ravi Prakash Reddy Nanga and Feliks Kogan. Our sincere thanks are also due to Drs. Weixia Liu and Steve Pickup for their imaging assistance as well as Ranjit Ittyerah and Dr. Damodar Reddy for their help with the animal model. This work was supported by the National Center for Research Resources and the National Institute of Biomedical Imaging and Bioengineering of the National Institutes of Health through grant number P41 EB015893, grant R21-DA032256 and the 3T program of the center for magnetic resonance research at University of Illinois at Chicago.

Abbreviations

^{1}H-MRS	proton magnetic resonance spectroscopy
Amares	advanced method for accurate, robust and efficient
APT	amide proton transfer
ATP	adenosine triphosphate
CEST	chemical exchange saturation transfer
CEST@2ppm	CEST peak located at +2ppm
DCE-MRI	dynamic contrast enhanced MRI
DS	direct saturation
FLASH	Fast Low-Angle SHot imaging
IACUC	institutional animal care and use committee
MRSI	magnetic resonance spectroscopic imaging
MT	magnetization transfer
MTR	magnetization transfer ratio
NOE	nuclear overhauser enhancement
PCr	phospho-creatine
PRESS	Point-RESolved Spectroscopy
ROI	region of interest
SE	Standard Error
VAPOR	VAriable Pulse power and Optimized Relaxation delays.

Reference

1. Bleyer WA. Epidemiologic impact of children with brain tumors. Child's nervous system. 1999; 15(11–12):758–763.
2. Panigrahy A, Bluml S. Neuroimaging of pediatric brain tumors: from basic to advanced magnetic resonance imaging (MRI). Journal of child neurology. 2009; 24(11):1343–1365. [PubMed: 19841424]
3. Lin A, Bluml S, Mamelak AN. Efficacy of proton magnetic resonance spectroscopy in clinical decision making for patients with suspected malignant brain tumors. Journal of neuro-oncology. 1999; 45(1):69–81. [PubMed: 10728912]
4. Wong ET, Jackson EF, Hess KR, Schomer DF, Hazle JD, Kyritsis AP, Jaeckle KA, Yung WK, Levin VA, Leeds NE. Correlation between dynamic MRI and outcome in patients with malignant gliomas. Neurology. 1998; 50(3):777–781. [PubMed: 9521274]
5. Li X, Lu Y, Pirzkall A, McKnight T, Nelson SJ. Analysis of the spatial characteristics of metabolic abnormalities in newly diagnosed glioma patients. Journal of magnetic resonance imaging. 2002; 16(3):229–237. [PubMed: 12205577]
6. Dean BL, Drayer BP, Bird CR, Flom RA, Hodak JA, Coons SW, Carey RG. Gliomas: classification with MR imaging. Radiology. 1990; 174(2):411–415. [PubMed: 2153310]
7. Watanabe M, Tanaka R, Takeda N. Magnetic resonance imaging and histopathology of cerebral gliomas. Neuroradiology. 1992; 34(6):463–469. [PubMed: 1436452]
8. Kondziolka D, Lunsford LD, Martinez AJ. Unreliability of contemporary neurodiagnostic imaging in evaluating suspected adult supratentorial (low-grade) astrocytoma. Journal of neurosurgery. 1993; 79(4):533–536. [PubMed: 8410222]
9. Ginsberg LE, Fuller GN, Hashmi M, Leeds NE, Schomer DF. The significance of lack of MR contrast enhancement of supratentorial brain tumors in adults: histopathological evaluation of a series. Surgical neurology. 1998; 49(4):436–440. [PubMed: 9537664]
10. Zhou J, Lal B, Wilson DA, Laterra J, van Zijl PC. Amide proton transfer (APT) contrast for imaging of brain tumors. Magnetic resonance in medicine. 2003; 50(6):1120–1126. [PubMed: 14648559]
11. van Zijl PC, Jones CK, Ren J, Malloy CR, Sherry AD. MRI detection of glycogen in vivo by using chemical exchange saturation transfer imaging (glycoCEST). Proceedings of the National Academy of Sciences of the United States of America. 2007; 104(11):4359–4364. [PubMed: 17360529]
12. Ling W, Regatte RR, Navon G, Jerschow A. Assessment of glycosaminoglycan concentration in vivo by chemical exchange-dependent saturation transfer (gagCEST). Proceedings of the National Academy of Sciences of the United States of America. 2008; 105(7):2266–2270. [PubMed: 18268341]
13. Haris M, Cai K, Singh A, Hariharan H, Reddy R. In vivo mapping of brain myo-inositol. Neuroimage. 2011; 54(3):2079–2085. [PubMed: 20951217]
14. Cai K, Haris M, Singh A, Kogan F, Greenberg JH, Hariharan H, Detre JA, Reddy R. Magnetic resonance imaging of glutamate. Nature Medicine. 2012; 18(2):302–306.
15. Nasrallah FA, Pages G, Kuchel PW, Golay X, Chuang KH. Imaging brain deoxyglucose uptake and metabolism by glucoCEST MRI. J Cereb Blood Flow Metab. 2013; 33(8):1270–1278. [PubMed: 23673434]
16. Xu HN, Nioka S, Glickson JD, Chance B, Li LZ. Quantitative mitochondrial redox imaging of breast cancer metastatic potential. Journal of biomedical optics. 2010; 15(3):036010. [PubMed: 20615012]
17. Jin T, Wang P, Zong X, Kim SG. Magnetic resonance imaging of the Amine-Proton EXchange (APEX) dependent contrast. Neuroimage. 2012; 59(2):1218–1227. [PubMed: 21871570]
18. Gilad AA, McMahon MT, Walczak P, Winnard PT Jr, Raman V, van Laarhoven HW, Skoglund CM, Bulte JW, van Zijl PC. Artificial reporter gene providing MRI contrast based on proton exchange. Nature biotechnology. 2007; 25(2):217–219.

19. Hua J, Jones CK, Blakeley J, Smith SA, van Zijl PC, Zhou J. Quantitative description of the asymmetry in magnetization transfer effects around the water resonance in the human brain. Magnetic resonance in medicine. 2007; 58(4):786–793. [PubMed: 17899597]
20. van Zijl PC, Yadav NN. Chemical exchange saturation transfer (CEST): what is in a name and what isn't? Magnetic resonance in medicine. 2011; 65(4):927–948. [PubMed: 21337419]
21. Jones CK, Polders D, Hua J, Zhu H, Hoogduin HJ, Zhou J, Luijten P, van Zijl PC. In vivo three-dimensional whole-brain pulsed steady-state chemical exchange saturation transfer at 7 T. Magnetic resonance in medicine. 2012; 67(6):1579–1589. [PubMed: 22083645]
22. Jin T, Wang P, Zong X, Kim SG. MR imaging of the amide-proton transfer effect and the pH-insensitive nuclear overhauser effect at 9.4 T. Magnetic resonance in medicine. 2012; 69(3):760–770. [PubMed: 22577042]
23. Zaiss M, Schmitt B, Bachert P. Quantitative separation of CEST effect from magnetization transfer and spillover effects by Lorentzian-line-fit analysis of z-spectra. Journal of magnetic resonance. 2011; 211(2):149–155. [PubMed: 21641247]
24. Zaiss, MW.; Schmitt, B.; Stieltjes, B.; Bachert, P. Enhancement of MT and CEST contrast via Heuristic fitting of Z-spectra. Proceedings of the 20th Annual Meeting ISMRM; Melbourne, Australia. 2012. p. 5136
25. Desmond KL, Moosvi F, Stanisz GJ. Mapping of amide, amine, and aliphatic peaks in the CEST spectra of murine xenografts at 7 T. Magnetic resonance in medicine. 2014; 71(5):1841–1853. [PubMed: 23801344]
26. Mori S, Eleff SM, Pilatus U, Mori N, van Zijl PC. Proton NMR spectroscopy of solvent-saturable resonances: a new approach to study pH effects in situ. Magnetic resonance in medicine. 1998; 40(1):36–42. [PubMed: 9660550]
27. van Zijl PC, Zhou J, Mori N, Payen JF, Wilson D, Mori S. Mechanism of magnetization transfer during on-resonance water saturation. A new approach to detect mobile proteins, peptides, and lipids. Magnetic resonance in medicine. 2003; 49(3):440–449. [PubMed: 12594746]
28. Jin T, Wang P, Zong X, Kim SG. Magnetic resonance imaging of the Amine-Proton EXchange (APEX) dependent contrast. NeuroImage. 2012; 59(2):1218–1227. [PubMed: 21871570]
29. Kim S, Pickup S, Hsu O, Poptani H. Diffusion tensor MRI in rat models of invasive and well-demarcated brain tumors. NMR in biomedicine. 2008; 21(3):208–216. [PubMed: 17530617]
30. O'Gorman RL, Michels L, Edden RA, Murdoch JB, Martin E. In vivo detection of GABA and glutamate with MEGA-PRESS: reproducibility and gender effects. Journal of magnetic resonance imaging. 2011; 33(5):1262–1267. [PubMed: 21509888]
31. Tkac I, Starcuk Z, Choi IY, Gruetter R. In vivo 1H NMR spectroscopy of rat brain at 1 ms echo time. Magnetic resonance in medicine. 1999; 41(4):649–656. [PubMed: 10332839]
32. Naressi A, Couturier C, Castang I, de Beer R, Graveron-Demilly D. Java-based graphical user interface for MRUI, a software package for quantitation of in vivo/medical magnetic resonance spectroscopy signals. Computers in biology and medicine. 2001; 31(4):269–286. [PubMed: 11334636]
33. Naressi A, Couturier C, Devos JM, Janssen M, Mangeat C, de Beer R, Graveron-Demilly D. Java-based graphical user interface for the MRUI quantitation package. Magnetic Resonance Materials in Physics, Biology and Medicine. 2001; 12(2–3):141–152.
34. Zhou J. Amide proton transfer imaging of the human brain. Methods Mol Biol. 2011; 711:227–237. [PubMed: 21279604]
35. Li AX, Hudson RH, Barrett JW, Jones CK, Pasternak SH, Bartha R. Four-pool modeling of proton exchange processes in biological systems in the presence of MRI-paramagnetic chemical exchange saturation transfer (PARACEST) agents. Magnetic resonance in medicine. 2008; 60(5):1197–1206. [PubMed: 18958857]
36. Cai K, Xu HN, Singh A, Moon L, Haris M, Reddy R, Li LZ. Breast Cancer Redox Heterogeneity Detectable with Chemical Exchange Saturation Transfer (CEST) MRI. Molecular imaging and biology. 2014
37. Cai K, Xu HN, Singh A, Haris M, Reddy R, Li LZ. Characterizing prostate tumor mouse xenografts with CEST and MT-MRI and redox scanning. Advances in experimental medicine and biology. 2013; 765:39–45. [PubMed: 22879012]

38. Walker EA, Fenton ME, Salesky JS, Murphey MD. Magnetic resonance imaging of benign soft tissue neoplasms in adults. Radiologic clinics of North America. 2011; 49(6):1197–1217. [PubMed: 22024295]
39. Ramani A, Dalton C, Miller DH, Tofts PS, Barker GJ. Precise estimate of fundamental in-vivo MT parameters in human brain in clinically feasible times. Magnetic resonance imaging. 2002; 20(10): 721–731. [PubMed: 12591568]
40. Mehta RC, Pike GB, Enzmann DR. Magnetization transfer magnetic resonance imaging: a clinical review. Topics in magnetic resonance imaging. 1996; 8(4):214–230. [PubMed: 8870180]
41. Warburg O. On the origin of cancer cells. Science. 1956; 123(3191):309–314. [PubMed: 13298683]
42. Ward K, Aletras A, Balaban R. A new class of contrast agents for MRI based on proton chemical exchange dependent saturation transfer (CEST). Journal of Magnetic Resonance. 2000; 143(1):79–87. [PubMed: 10698648]
43. Haris M, Nanga RP, Singh A, Cai K, Kogan F, Hariharan H, Reddy R. Exchange rates of creatine kinase metabolites: feasibility of imaging creatine by chemical exchange saturation transfer MRI. NMR in biomedicine. 2012; 25(11):1305–1309. [PubMed: 22431193]
44. Singh, A.; Haris, M.; Cai, K.; Hariharan, H.; Reddy, R. Chemical Exchange Transfer Imaging of Creatine. Proceedings of the 20th Annual Meeting ISMRM; Melbourne, Australia. 2011. p. 4619
45. Sun PZ, Benner T, Kumar A, Sorensen AG. Investigation of optimizing and translating pH-sensitive pulsed-chemical exchange saturation transfer (CEST) imaging to a 3T clinical scanner. Magnetic resonance in medicine. 2008; 60(4):834–841. [PubMed: 18816867]
46. Arus C, Barany M, Westler WM, Markley JL. 1H NMR of intact muscle at 11 T. FEBS letters. 1984; 165(2):231–237. [PubMed: 6607178]
47. Middleton DA, Hockings PD, Glen S, Reid DG, Rose SE, Crozier S, Roffman W, Rothaul AL, Hunter AJ, Doddrell DM. Image directed proton spectroscopy of gerbil brain at 7 tesla. NMR in biomedicine. 1995; 8(3):118–126. [PubMed: 8579999]
48. Haris M, Singh A, Cai K, Kogan F, McGarvey J, Debrosse C, Zsido G, Witschey W, Koomalsingh K, Pilla J, Chirinos J, Ferrari V, Gorman J, Hariharan H, Gorman R, Reddy R. A novel technique for in vivo mapping of myocardial creatine kinase metabolism. Nature Medicine. 2014; 20:209–214.
49. Kuszewski JJ, Thottungal RA, Clore GM, Schwieters CD. Automated error-tolerant macromolecular structure determination from multidimensional nuclear Overhauser enhancement spectra and chemical shift assignments: improved robustness and performance of the PASD algorithm. Journal of biomolecular NMR. 2008; 41(4):221–239. [PubMed: 18668206]
50. Stadlbauer A, Gruber S, Nimsky C, Fahlbusch R, Hammen T, Buslei R, Tomandl B, Moser E, Ganslandt O. Preoperative grading of gliomas by using metabolite quantification with high-spatial-resolution proton MR spectroscopic imaging. Radiology. 2006; 238(3):958–969. [PubMed: 16424238]
51. Belitzer V, Tsybakova E. About mechanism of phosphorylation, respiratory coupling. Biochimia. 1939; 4:516–533.
52. Usenius JP, Vainio P, Hernesniemi J, Kauppinen RA. Choline-containing compounds in human astrocytomas studied by 1H NMR spectroscopy in vivo and in vitro. Journal of neurochemistry. 1994; 63(4):1538–1543. [PubMed: 7931308]
53. Chang L, McBride D, Miller BL, Cornford M, Booth RA, Buchthal SD, Ernst TM, Jenden D. Localized in vivo 1H magnetic resonance spectroscopy and in vitro analyses of heterogeneous brain tumors. Journal of neuroimaging. 1995; 5(3):157–163. [PubMed: 7626823]
54. Peeling J, Sutherland G. High-resolution 1H NMR spectroscopy studies of extracts of human cerebral neoplasms. Magnetic resonance in medicine. 1992; 24(1):123–136. [PubMed: 1556919]
55. Yerli H, Agildere AM, Ozen O, Geyik E, Atalay B, Elhan AH. Evaluation of cerebral glioma grade by using normal side creatine as an internal reference in multi-voxel 1H-MR spectroscopy. Diagnostic and interventional radiology. 2007; 13(1):3–9. [PubMed: 17354186]
56. Sun PZ, Sorensen AG. Imaging pH using the chemical exchange saturation transfer (CEST) MRI: Correction of concomitant RF irradiation effects to quantify CEST MRI for chemical exchange rate and pH. Magnetic resonance in medicine. 2008; 60(2):390–397. [PubMed: 18666128]

57. Goerke S, Zaiss M, Bachert P. Characterization of creatine guanidinium proton exchange by water-exchange (WEX) spectroscopy for absolute-pH CEST imaging in vitro. NMR in biomedicine. 2014; 27(5):507–518. [PubMed: 24535718]

58. Chappell MA, Donahue MJ, Tee YK, Khrapitchev AA, Sibson NR, Jezzard P, Payne SJ. Quantitative Bayesian model-based analysis of amide proton transfer MRI. Magnetic resonance in medicine. 2013; 70(2):556–567. [PubMed: 23008121]

59. Zaiss M, Xu J, Goerke S, Khan IS, Singer RJ, Gore JC, Gochberg DF, Bachert P. Inverse Z-spectrum analysis for spillover-, MT-, and T1 -corrected steady-state pulsed CEST-MRI--application to pH-weighted MRI of acute stroke. NMR in biomedicine. 2014; 27(3):240–252. [PubMed: 24395553]

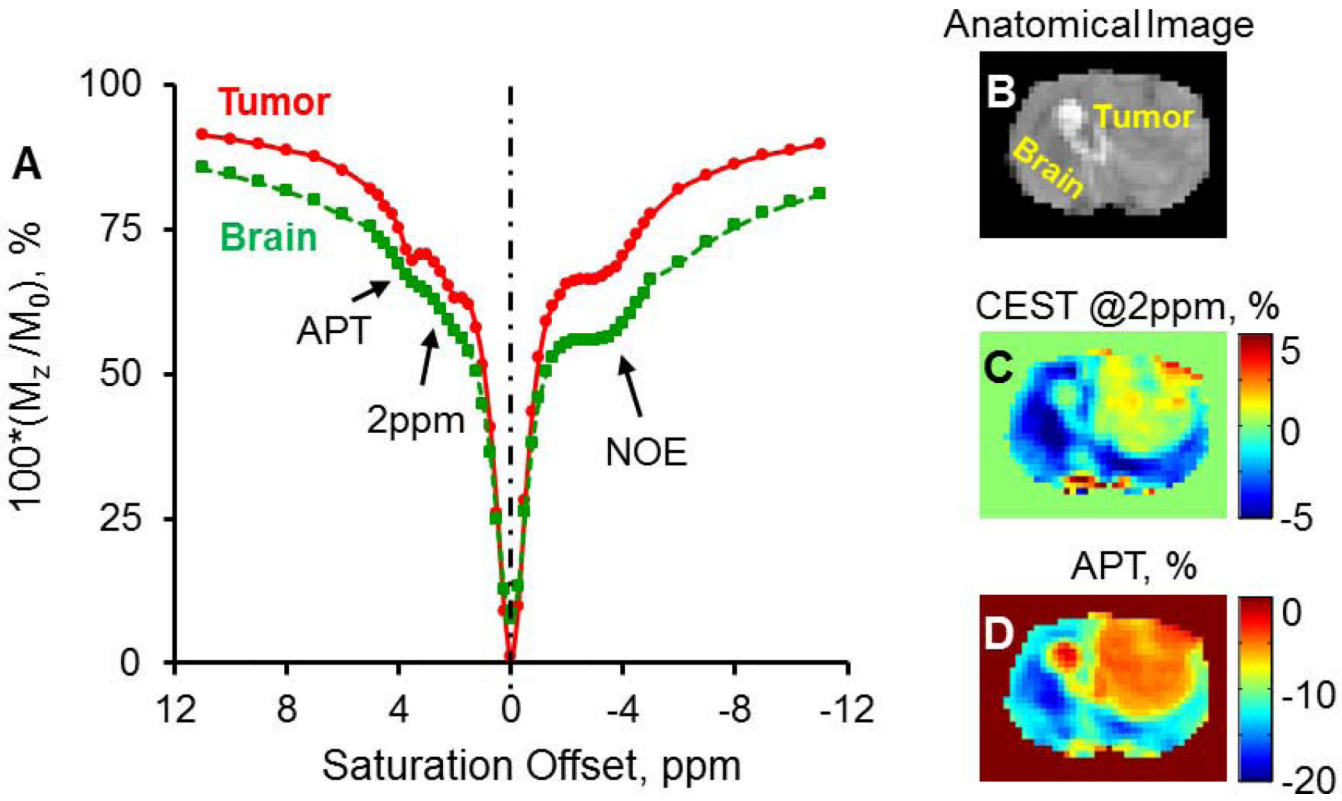

Figure 1.

Representative Z-spectra (50 Hz, 3s) from normal brain (A, green) and brain tumor (A, red, 4 weeks) show visible CEST peaks for bulk water, APT, aliphatic NOE, CEST@2ppm and the underlying MT. B–D) show the anatomical image (B), the corresponding CEST@2ppm (C) and APT (D) maps that are quantified based on MTR asymmetry. Negative contrasts were detected from most of the brain region by using this conventional method.

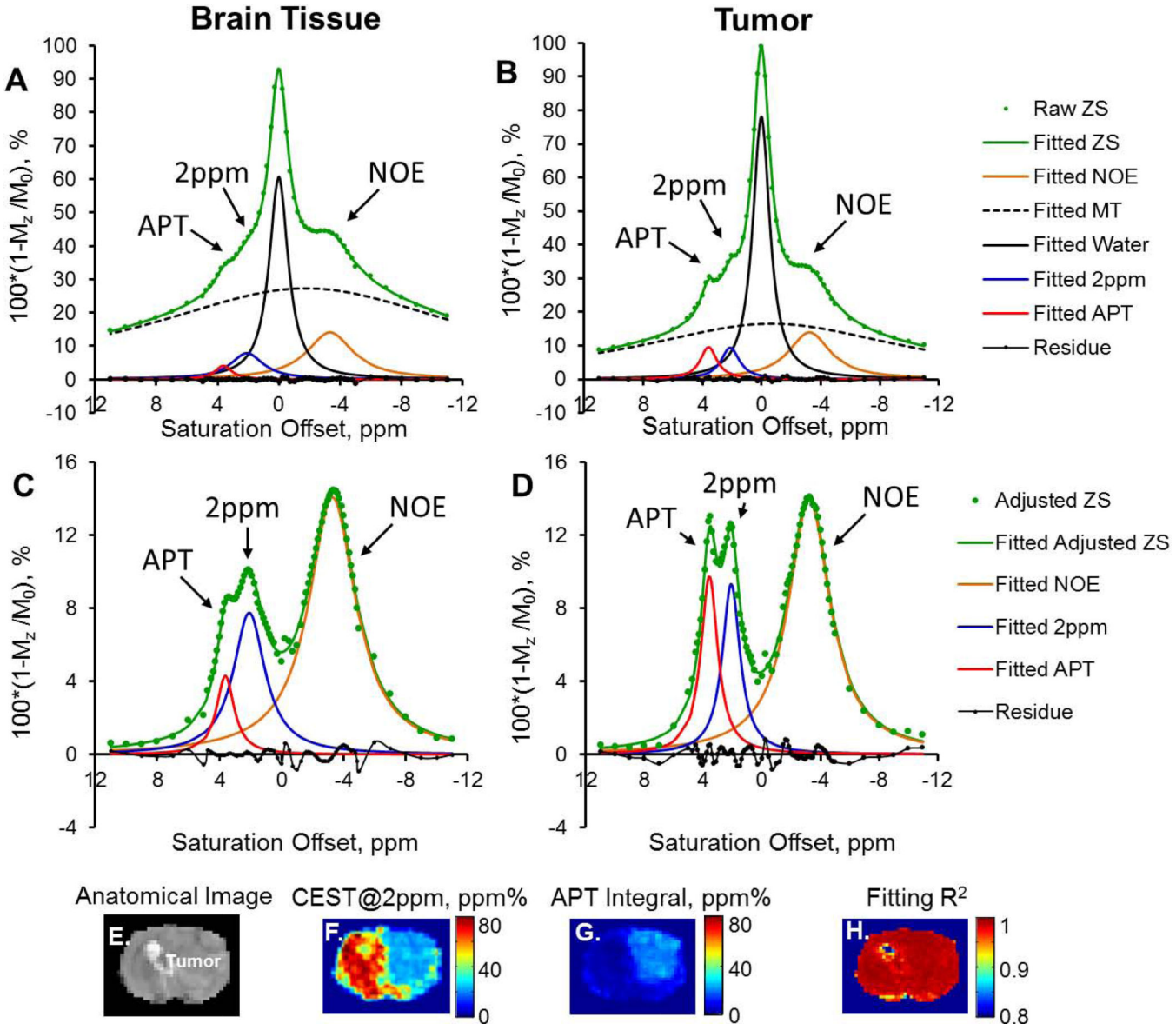

Figure 2.

Z-spectra (ZS), scaled upside down, from normal brain (Left column) and brain tumor (Right column) were fitted with a sum of five Lorentzian functions (A and B). Water DS and MT were then subtracted from the entire Z-spectra (adjusted ZS) for a secondary fitting of NOE, CEST@2ppm and APT (C and D). The anatomic image (E), pixel-wise fitted CEST@2ppm (F), APT (G) maps, and the corresponding R^2 map are shown from E to H.

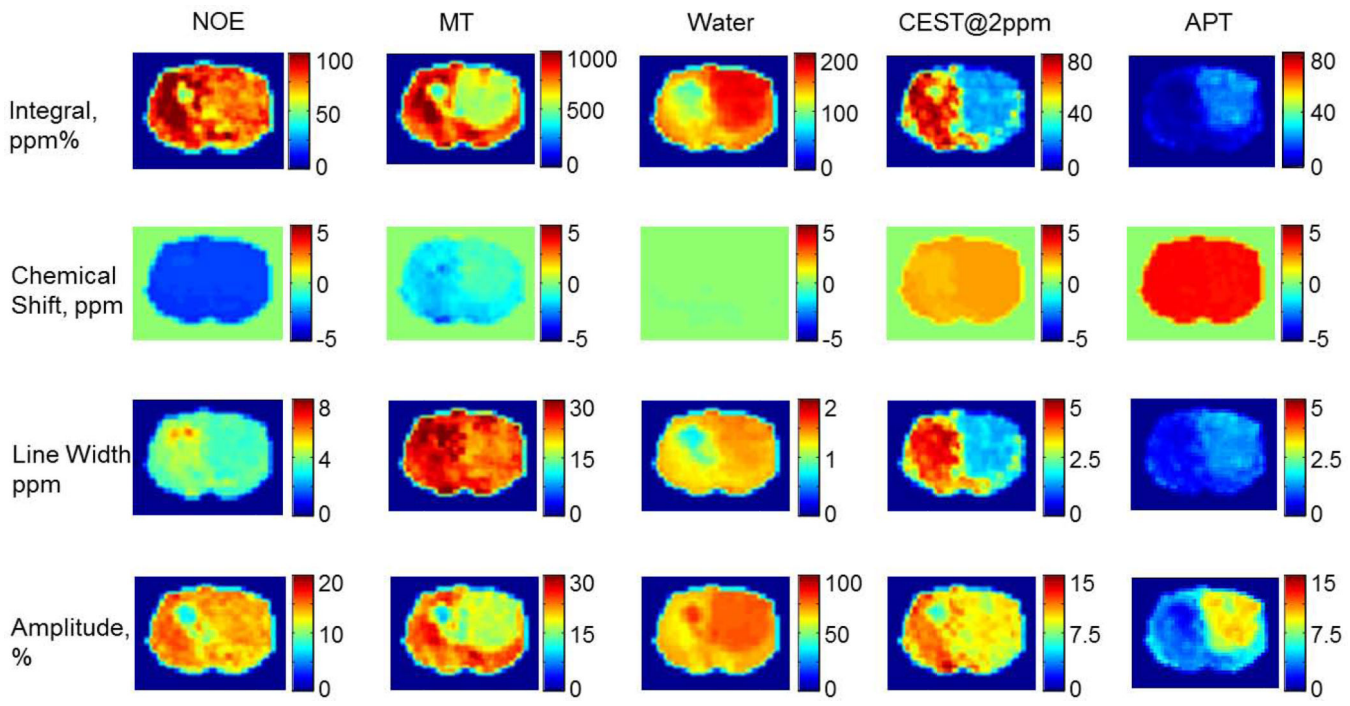

Figure 3.

Pixel-by-pixel fitted integral, chemical shift, linewidth and amplitude maps of the five components contributing to the Z-spectra (50 Hz, 3s) of the representative tumor brain.

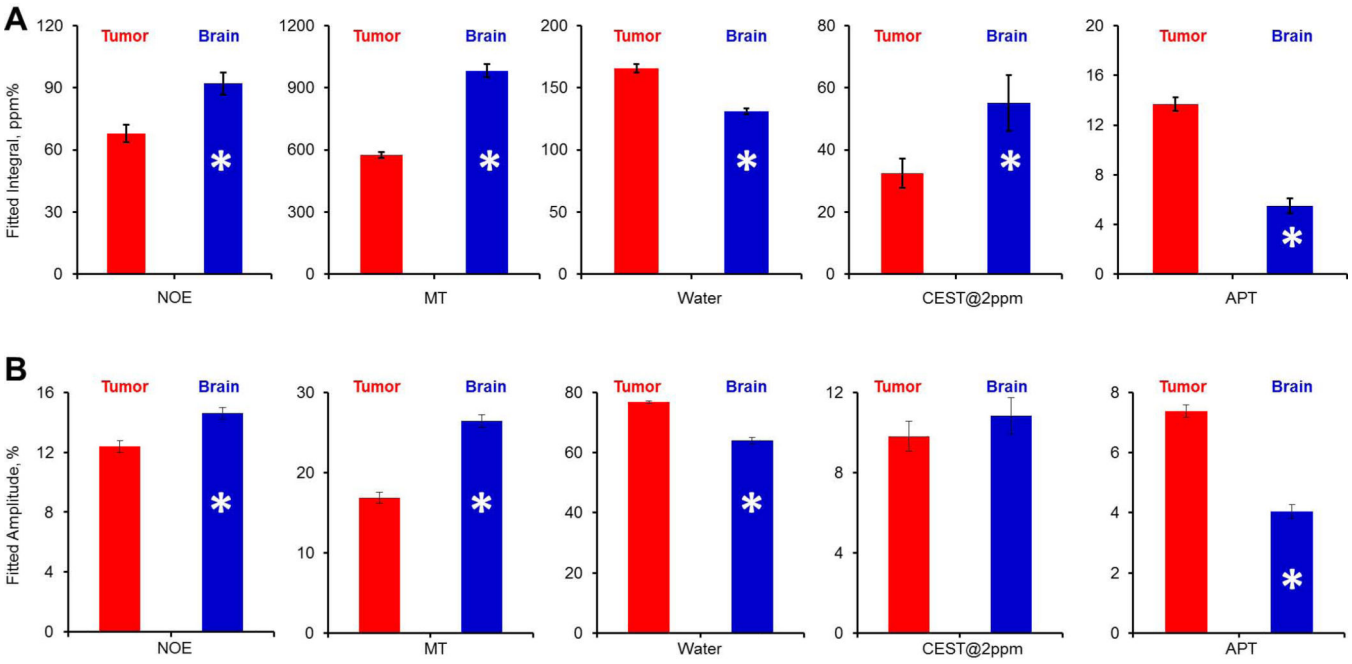

Figure 4.

The summary of the fitted peak integrals and amplitudes from brain tumor (red) and normal brain tissue (blue). From left to right are NOE, MT, Water, CEST@2ppm and APT respectively. *p<0.05.

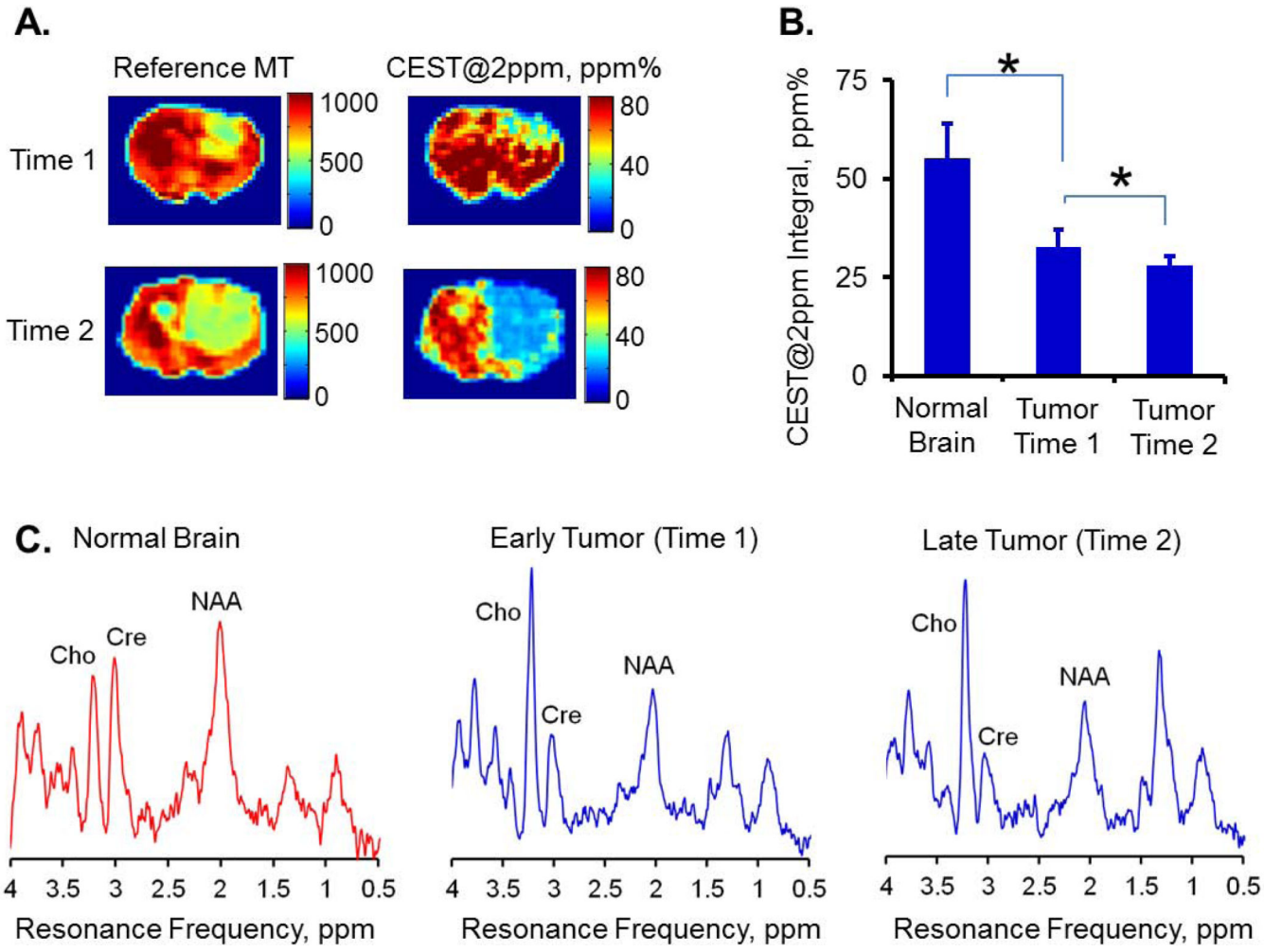

Figure 5.

The CEST@2ppm integral decreased in tumor compared to normal brain tissue and further reduced with tumor progression (A and B). Similar trend holds with the creatine change detected by MR spectroscopy (C). The summed MR spectra of each group were first normalized with the corresponding water reference signals. The normal brain data was taken from the first imaging time point. The reference MT maps (A) help to localize brain tumors. Cho: Choline, Cre: Creatine, NAA: N-Acetylaspartic Acid.

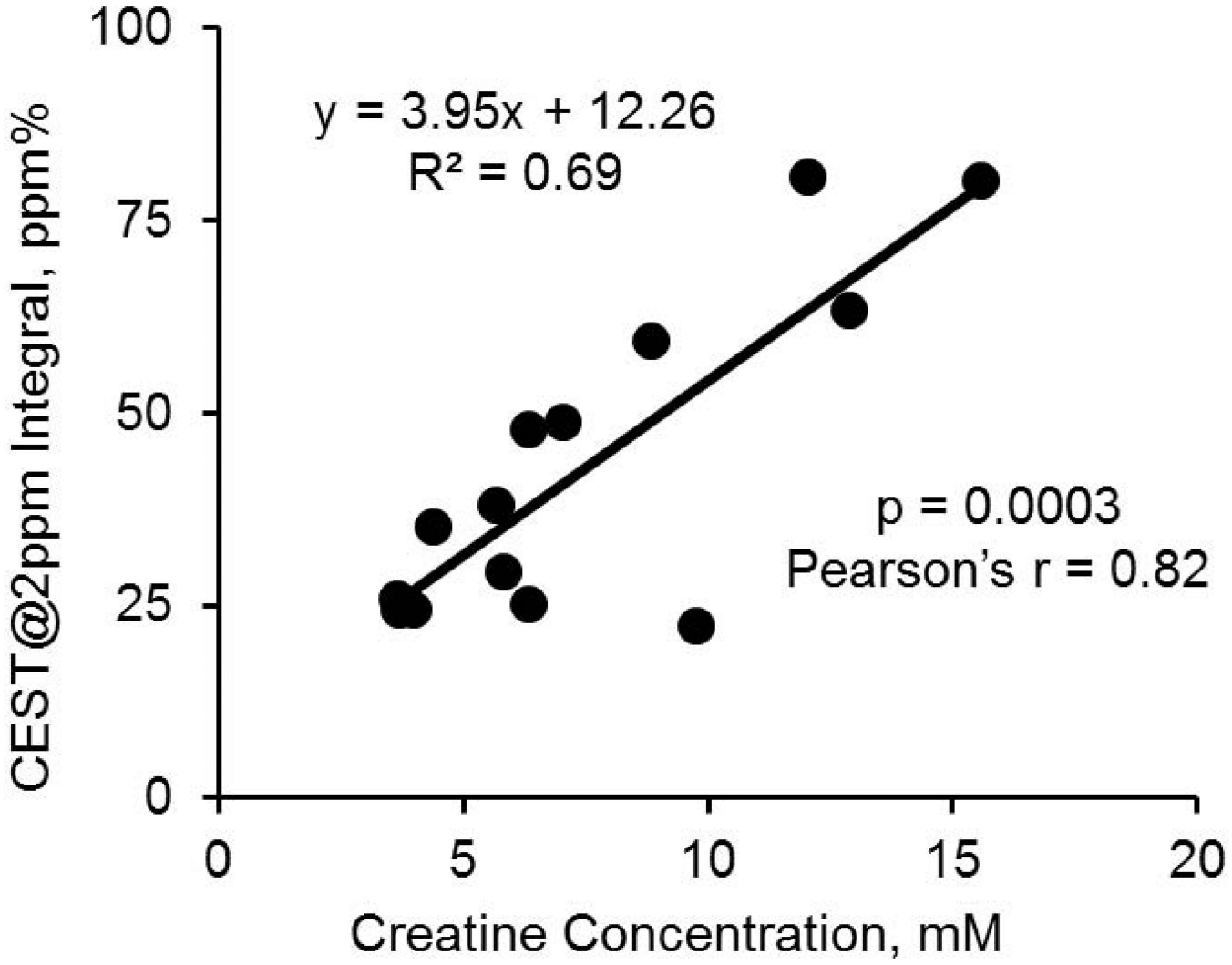

Figure 6.

The linear correlation of the CEST@2ppm integrals from individual tumors and normal brain tissues (as Figure 5B) with their corresponding creatine concentrations quantified with MR spectroscopy.

Table 1

List of the initial and fitted values of the amplitudes, frequency offsets and linewidths of the five components contributing to Z spectra shown in Figure 1 and 2.

Parameters	Initial values*	Fitted values for brain ROI*	Fitted values for tumor ROI*
Frequency offset, ppm	−3.23, −1.48,0.02,2.04,3.63	−3.33, −1.76,0.02,2.10,3.63 −3.28,-------,-------,2.08,3.62	−3.24, −0.67,0.02,2.12,3.59 −3.24,-------,-------,2.09,3.58
Linewidth, ppm	4.28,27.43,1.35,2.23,1.49	3.67,25.62,1.49,2.59,1.32 3.71,-------,-------,2.49,1.38	3.43,22.19,1.40,1.52,1.38 3.48,-------,-------,1.47,1.40
Amplitude, %	15.05,20.3,71.00,9.51,6.21	14.07,27.28,60.72,7.87,4.11 14.07,-------,-------, 7.75,4.30	13.96,16.53,78.18,9.43,9.58 13.92,-------,-------,9.33,9.75

* From left to right: NOE, MT, Water, 2ppm peak and APT; the 1st row: the first order of fitting; the 2nd row: the secondary fitting. MT and water peaks were not fitted (labeled as "-------") in the secondary fitting.